J Therm Anal Calorim (2015) 121:1003–1010
DOI 10.1007/s10973-015-4510-7

Fine $MnFe_2O_4$ nanoparticles for potential environmental applications

Synthesis and characterization

Marcela Stoia · Cornelia Muntean · Bogdan Militaru

Received: 20 October 2014 / Accepted: 29 January 2015 / Published online: 1 March 2015

Abstract Manganese ferrite nanopowder was prepared by the thermal decomposition of gels obtained from manganese, iron nitrates, and polyvinyl alcohol. The evolution of the gels during the thermal treatment was studied by means of thermal analysis and FT-IR spectrometry. X-ray diffractometry evidenced that manganese ferrite can be obtained as single crystalline phase at temperatures lower than 500 °C. Starting with 500 °C, a secondary phase containing Mn(III) appears, while the annealing at 700 and 1,000 °C leads to $Mn_{0.176}Fe_{1.824}O_3$ and $(Fe_{0.42}Mn_{0.58})_2O_3$, where Mn is at oxidation state (III). The decomposition of manganese ferrite was evidenced also by TG/DSC combined technique of the powder obtained at 400 °C, containing $MnFe_2O_4$ as single crystalline phase. Scanning electron microscopy images evidenced the formation of very fine spherical particles ($d < 15$ nm) of manganese ferrite, in case of the sample annealed at 400 °C. This powder showed good catalytic activity for the oxidative degradation of phenol, in the presence of peroxydisulfate as oxidant agent, so it might be considered a promising nanomaterial for environmental applications.

Keywords Manganese ferrite · Nanoparticles · Polyvinyl alcohol · Thermal decomposition

Introduction

In the last years, nanoscale spinel ferrites have drawn major attention because of their technological applications in magnetic recording, ferrofluids, and catalysts [1]. The reduced size and the effects of magnetic interactions between nanoparticles give to these nanoferrites different characteristics in comparison with the bulk material [1]. Superparamagnetic spinel ferrites MFe_2O_4 (M = Mn, Fe, Co, Ni) are currently considered among the most promising magnetic nanoparticles in medical applications for contrast enhancement in magnetic resonance imaging (MRI), magnetical drug delivery, and hyperthermia cancer therapy [2]. One of magnetic ferrites applications extensively studied in the last decade is the removal from wastewater of heavy metals [3] and of very toxic organic pollutants (e.g., phenol and its derivatives) [4] that can cause considerable damage and threat to the ecosystem and to the human health even at low concentrations.

Manganese ferrite is a magnetic ferrite with cubic spinel structure, which has been used in various technological applications (magnetic materials, gas sensor, and absorbent material for hot gas) [5–7]. The properties of manganese ferrite depend on the composition, morphology, and size, which are strongly related to the synthesis parameters [8]. Several methods have been developed to synthesize $MnFe_2O_4$ nanoparticles, such as solid-phase reactions [9, 10], mechanical ball-milling [11], thermal decomposition [12], hydrothermal [13], coprecipitation [14], combustion [15], and microemulsion method [16]. It was reported that at elevated temperatures, $MnFe_2O_4$ is unstable in air and Mn^{2+} ions on the surface oxidize to form Mn^{3+} ions resulting in the dissociation of the formed $MnFe_2O_4$. Thus, it was concluded that any preparation method involving a calcination step is not suitable for the preparation of manganese ferrite nanoparticles [15].

Nanosized manganese ferrite was reported to be a promising material for environmental applications, as adsorbent material for different inorganic and organic

M. Stoia (✉) · C. Muntean · B. Militaru
Faculty of Industrial Chemistry and Environmental Engineering, Research Institute for Renewable Energy, Politehnica University Timisoara, 6 Pîrvan Blv., 300223 Timisoara, Romania
e-mail: marcela.stoia@upt.ro

pollutants [5, 17] as well as catalyst for pollutants degradation [18, 19]. It was also reported that $MnFe_2O_4$ presents high activity in activating peroxymonosulfate (PMS) to produce sulfate radicals for degradation of organic dyes and could be separated with a magnet without any loss [20].

In this paper, we report the obtaining of manganese ferrite as very fine nanoparticles, by thermal decomposition of the precursor formed between metal nitrates and polyvinyl alcohol (PVA). Thermal analysis has been used to characterize the precursor and the powders annealed at different temperatures, in order to evidence the evolution of the oxidic system with the annealing temperature. $MnFe_2O_4$ nanopowder obtained at 400 °C was tested as catalyst for the oxidative degradation of phenol, in the presence of peroxydisulfate anion as oxidant.

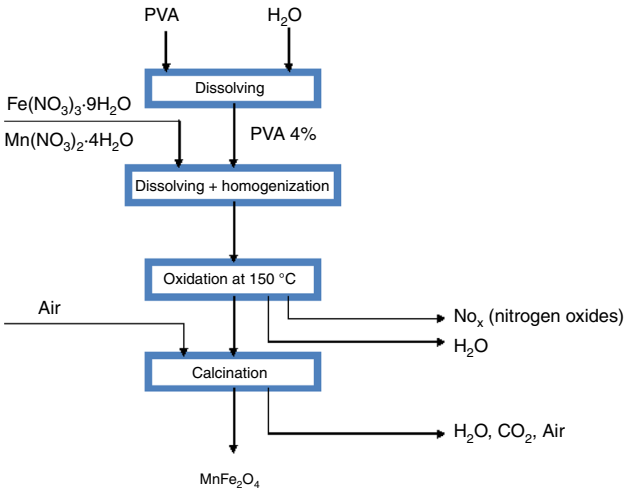

Scheme 1 Stages of obtaining manganese ferrite from metal nitrates and PVA

Experimental

Materials and methods

The reagents used in synthesis and catalysis experiments were of analytical grade and were used without further purification: $Mn(NO_3)_2{\cdot}4H_2O$, $Fe(NO_3)_3{\cdot}9H_2O$, PVA ($M = 60{,}000$ g mol^{-1}), phenol C_6H_5-OH, potassium peroxydisulfate $K_2S_2O_8$, nitric acid HNO_3, and sodium hydroxide NaOH.

In a typical synthesis, the necessary amount of manganese nitrate is dissolved in a 4 % PVA aqueous solution, calculated for a molar ratio PVA (monomer) : NO_3^- = 1:1. The solution was kept under stirring for an hour, then was slowly heated up to 100 °C, and kept at this temperature until it became a gel. The temperature was finally increased up to 140 °C where the sample was kept for 8 h, in order to complete the redox reaction between PVA and metal nitrates. The precursor powder obtained was further calcined at 300, 400, 500, 700, and 1,000 °C. The synthesis procedure is shown in Scheme 1. All powders were characterized by combined TG/DTA techniques, FT-IR spectroscopy, XRD analysis, SEM microscopy, and magnetic measurements.

Characterization techniques

Thermal behavior of the precursor was studied using a 1500 D MOM Budapest derivatograph, in static air atmosphere in the range of 25–1,000 °C with a heating rate of 10 °C min^{-1}, using alumina crucibles. Thermal behavior study of the powders calcined at 300 and 400 °C was performed on a Netzsch STA 449C thermobalance, in air atmosphere at a flow rate of 20 cm^3 min^{-1}. The TG/DSC curves were recorded in the temperature range 25–1,000 °C with a heating rate of 10 °C min^{-1}, using alumina crucibles.

The phase composition of the samples was determined by XRD, using a Rigaku Ultima IV diffractometer ($Cu_{K\alpha}$ radiation). Crystallite size was calculated using the whole-pattern profile-fitting method (WPPF). The instrument influence was subtracted using the diffraction pattern of a Si standard recorded in the same conditions as the patterns of the samples. FT-IR spectra were recorded using a Shimadzu Prestige-21 spectrometer in the range 400–4,000 cm^{-1}, using KBr pellets and a resolution of 4 cm^{-1}. The morphology of the nanopowders was investigated by scanning electron microscopy (SEM), using a FEI Quanta FEG 250 microscope (at 30 kV and working distance of 5 mm). The behavior in external magnetic field of the obtained nanopowders was studied using an installation equipped with a data acquisition system [21].

Results and discussion

Due to the difficulties in the obtaining of manganese ferrite, generated by the easy modification of manganese oxidation state, we started the study regarding the obtaining of $MnFe_2O_4$ from iron and manganese nitrates and PVA with the study of the interaction between manganese nitrate and PVA. In our previous studies [22], we showed that iron(III) nitrate interacts with PVA forming some coordination compounds with PVA oxidation products, generally carboxylate anions, used as precursors for iron oxides. By thermal decomposition of this precursor at temperatures up to 400 °C, γ-Fe_2O_3 is obtained as major crystalline phase, while at temperatures higher than 500 °C, α-Fe_2O_3 is

obtained. The formation of the spinelic γ-Fe_2O_3 phase favors the obtaining of spinelic ferrite, if the M (II) oxide (MO) forms also at low temperatures.

In case of manganese ferrite formation, the determining factor is the nature of manganese oxide resulting from the thermal decomposition of the precursor (formed in the redox interaction between manganese(II) nitrate and PVA).

In order to see how the involved metal nitrates ($Fe(NO_3)_3$ and $Mn(NO_3)_2$) and their mixture interact with PVA, we prepared solutions of each nitrate with PVA (molar ratio 1:1 as in the synthesis). The samples were named MnPVA, FePVA, and MnFePVA. These solutions have been heated at 60 °C until they became gels (around 4 h). The obtained gels (MnPVA, FePVA and MnFePVA) have been studied by thermogravimetric (TG) and differential thermal analysis (DTA). The registered thermoanalytical curves are presented in Fig. 1a–c.

From the evolution of TG and DTA curves in case of MnPVA gel (Fig. 1a), it results that, after the endothermic dehydration of the gel, which occurs up to 170 °C, there are two exothermic processes. The first one, accompanied by a fast mass loss of $\sim$16 % and a sharp exothermic effect with maximum at 210 °C, can be assigned to the interaction of manganese nitrate with PVA and the burning of the formed precursor; the remaining organic residue further burns around 280 °C. Thus, around 300 °C the thermal decomposition of the precursor is complete.

In case of the FePVA gel, we clearly see the redox interaction of iron nitrate with PVA, around 180 °C, as the first weak exothermic process, with formation of iron carboxylates compounds that further burn in the range 250–350 °C, generating a large exothermic effect.

When a mixture of the two metal nitrates is present in the PVA gel, the thermal behavior is different from that of the individual ones. The redox interaction of nitrate ions with PVA takes place around 190 °C, followed by the combustion of the formed precursor in one step, which finishes at 300 °C. Thus the presence of Fe^{3+}, which forms relatively stable carboxylate compounds in interaction with PVA, stabilizes the system, allowing the formation of intermediary compounds, which further decompose to the oxidic system. On the other hand, the presence of Mn^{2+} ions promotes, through their catalytic activities, the thermal decomposition of the formed Fe(III) and Mn(II) carboxylates.

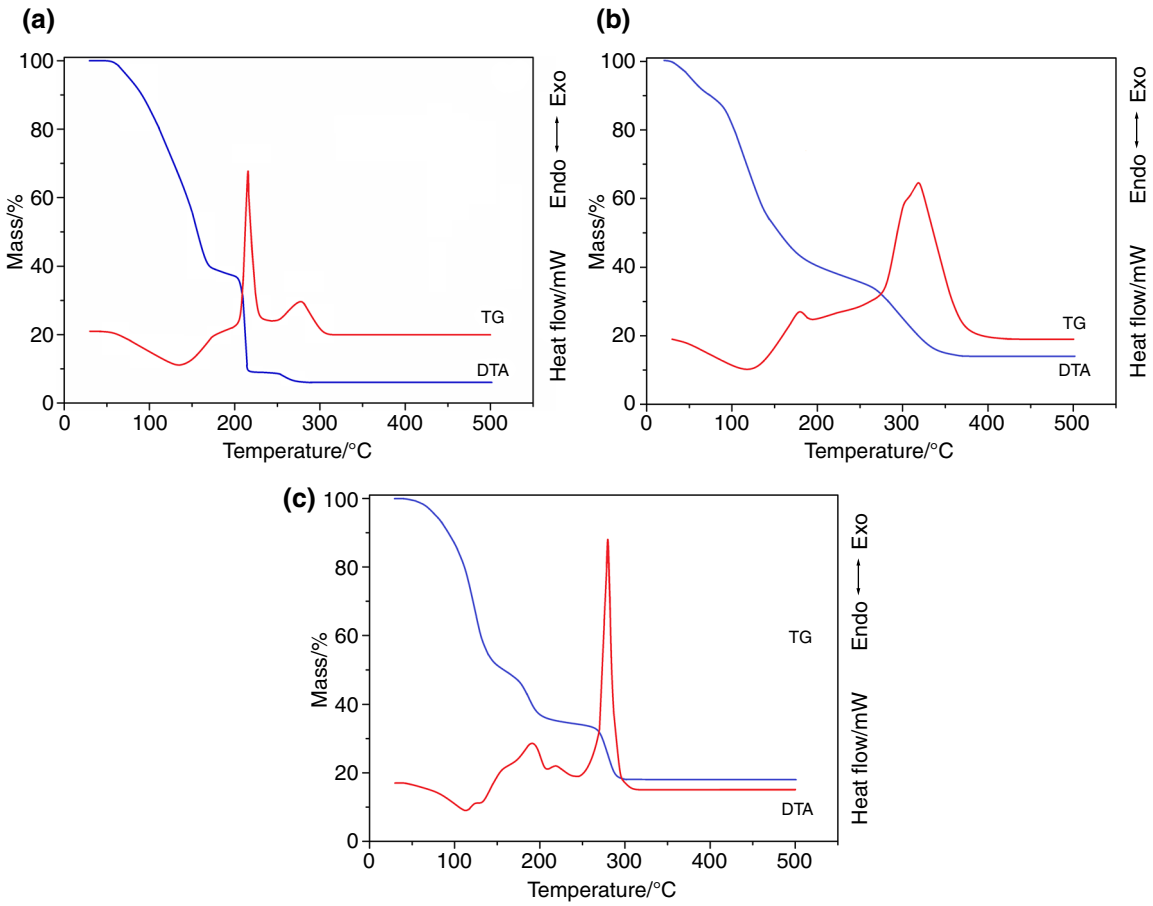

Fig. 1 TG and DTA curves of the gels: **a** MnPVA; **b** FePVA; **c** MnFePVA

In order to complete the redox reaction between NO_3^- ions and PVA and to obtain the corresponding oxide precursor, the MnPVA, FePVA, and MnFePVA gels were kept at 180 °C for 6 h. The obtained products, with spongeous aspect (voluminous, porous structure) were grinded into fine powders. In case of MnPVA gel, a self-propagating combustion took place, leading to a black fluffy product, confirming the conclusion of thermal analysis. The powders obtained at 180 °C were characterized by FT-IR spectrometry. Figure 2 presents the FT-IR spectra of initial gels (Fig. 2a) and of the powders obtained after thermal treatment at 180 °C (Fig. 2b).

During the drying process at 60 °C, FePVA gel showed some gas emissions, suggesting that the redox reaction has already started. This was also proved by the presence in the FT-IR spectrum of two bands characteristic to COO^- and COOH groups (1,672 and 1,568 cm^{-1}) resulting from the oxidation of $–CH_2$-OH groups [22]. The presence of the strong band located at 1,381 cm^{-1} may be due to the presence of the unreacted NO_3^- overlapped with the band generated by the symmetric stretching vibrations of COO^- groups. Bands characteristic to C–OH bonds in PVA are present in the range 900–1,100 cm^{-1}. The MnPVA gel exhibits more intense bands characteristic to PVA gel (848, 1,037, 1,697, 1,749, 2,800–3,000, 3,600–3,700 cm^{-1} [23]). The presence of manganese nitrate is less visible in the FT-IR spectrum.

After thermal treatment at 180 °C in the corresponding FT-IR spectra (Fig. 2), the formation of metal carboxylates was evidenced through the characteristic bands (ν_{sim}(COO) and ν_{ass} (COO)) only in case of FePVA sample (1,552 and 1,386 cm^{-1}) and MnFePVA sample (shoulder around 1,550 cm^{-1} and the band located at 1,305 cm^{-1}). In case of MnPVA sample, the FT-IR spectrum exhibits only the bands characteristic to the adsorbed water molecules (3,441 and 1,629 cm^{-1}) and the bands characteristic to Mn–O bonds, confirming the burning of the organic part and the formation of the corresponding manganese oxide. According to the literature, the two bands located at 503 and 623 cm^{-1} are characteristic to Mn_3O_4 [24, 25].

In order to establish the temperature at which the thermal decomposition of manganese ferrite precursor (MnFePVA) obtained at 180 °C finishes, we have studied its thermal behavior (Fig. 3). Both TG and DTA curves show that the redox reaction between nitrate ions and PVA was almost finished (a smaller mass loss was recorded around 200 °C associated with a very weak exothermic effect). The combustion of the formed precursor finishes around 325 °C. Thus, we have chosen to calcinate the precursor at different temperatures, starting with 300 °C.

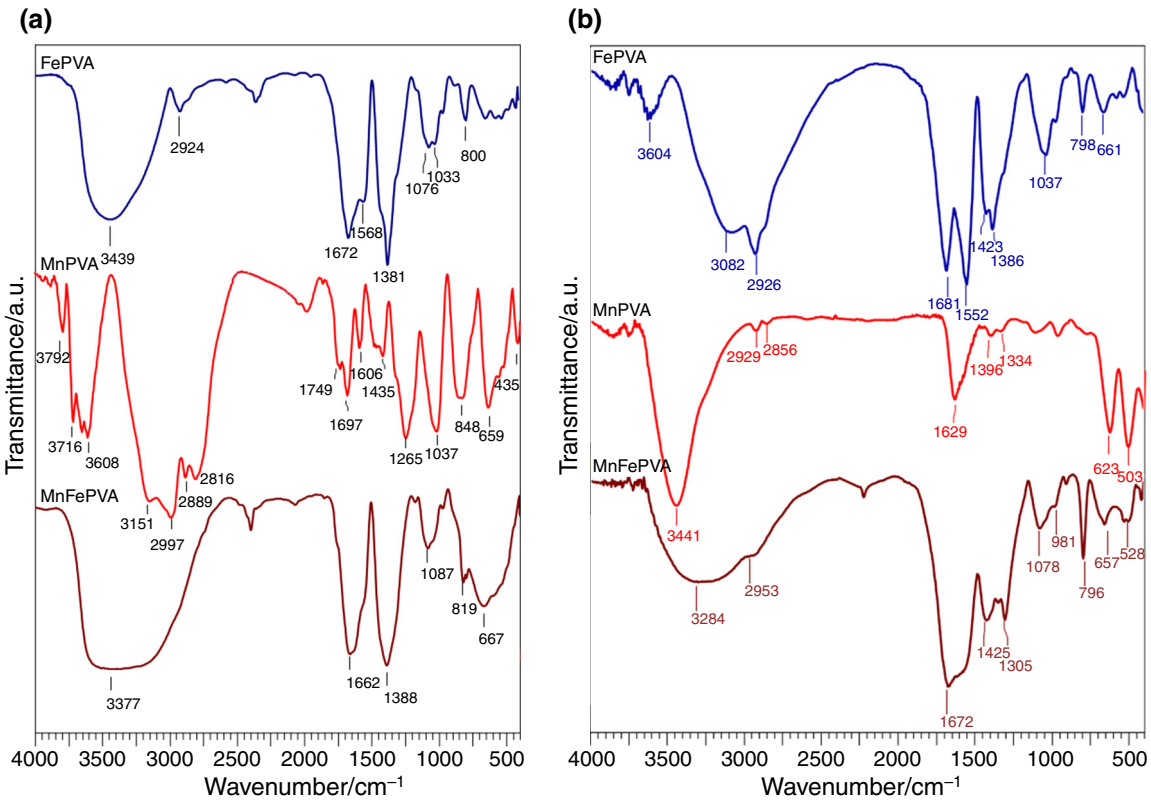

Fig. 2 FT-IR spectra of the gels FePVA, MnPVA, and FeMnPVA (**a**) and the powders obtained at 180 °C (**b**)

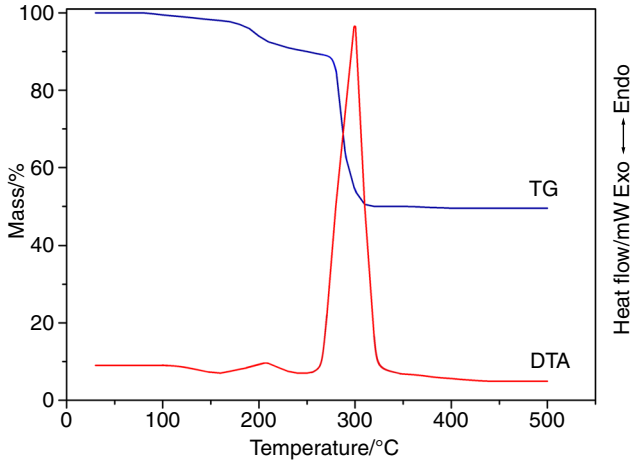

Fig. 3 TG and DTA curves of manganese ferrite precursor (MnFePVA)

Usually, the manganese ferrite was reported to be obtained at low temperatures (up to 200 °C) from wet methods [2, 26, 27]. The only reported synthesis method that leads to manganese ferrite at higher temperatures is the combustion method [28]. When the ferrite is obtained at low temperatures, where the crystallinity of the product is low, it might be possible to have individual oxides with spinelic structure. In order to facilitate the crystallization of the phases, we chose a long calcination time (6 h).

The XRD patterns of the powders annealed at different temperatures are shown in Fig. 4a. The data derived from XRD analysis are given in Table 1. From these data, one may notice that cubic $MnFe_2O_4$ is present in all samples. As the annealing temperature increases, the average size of the crystallites increases from 2 to 21 nm, and the proportion in the sample decreases from 100 % at 300 and 400 °C to 6–7 % at 700 and 1,000 °C. The lattice parameter (a) also increases with temperature, and at 700 and 1,000 °C the value (8.499 Å) is close to the one in the JCPDS (Joint Committee on Powder Diffraction Standards) file (8.498 Å).

In the sample annealed at 500 °C, $MnFe_2O_4$ is still the main phase (72 %) but rhombohedral $Mn_{0.176}Fe_{1.824}O_3$ appears as secondary phase. $Mn_{0.176}Fe_{1.824}O_3$ becomes the main phase at 700 °C (65 %), while at 1,000 °C, its proportion decreases to 25 %. At this temperature, the main phase is cubic $(Fe_{0.42}Mn_{0.58})_2O_3$ (68 %) which was also present in the sample annealed at 700 °C, in a smaller proportion (29 %). For $Mn_{0.176}Fe_{1.824}O_3$ the values of the lattice parameter slightly increased from 500 to 1,000 °C, remaining close to the ones in the JCPDS file ($a = b = 5.031$ Å; $c = 13.716$ Å) at all temperatures.

In order to understand the evolution of the crystalline phases in this system, we have also shown the XRD patterns of the individual iron oxides (Fig. 4b) and manganese oxides (Fig. 4c), obtained from the gels FePVA and MnPVA under the same thermal treatment as FeMnPVA gel. The XRD pattern of the powder MnFePVA annealed at 300 °C evidences a weak crystallization degree, only some broad diffraction peaks being present. By annealing the precursor MnFePVA at 400 °C for 6 h, the spinelic crystalline phase becomes better crystallized. Comparing the

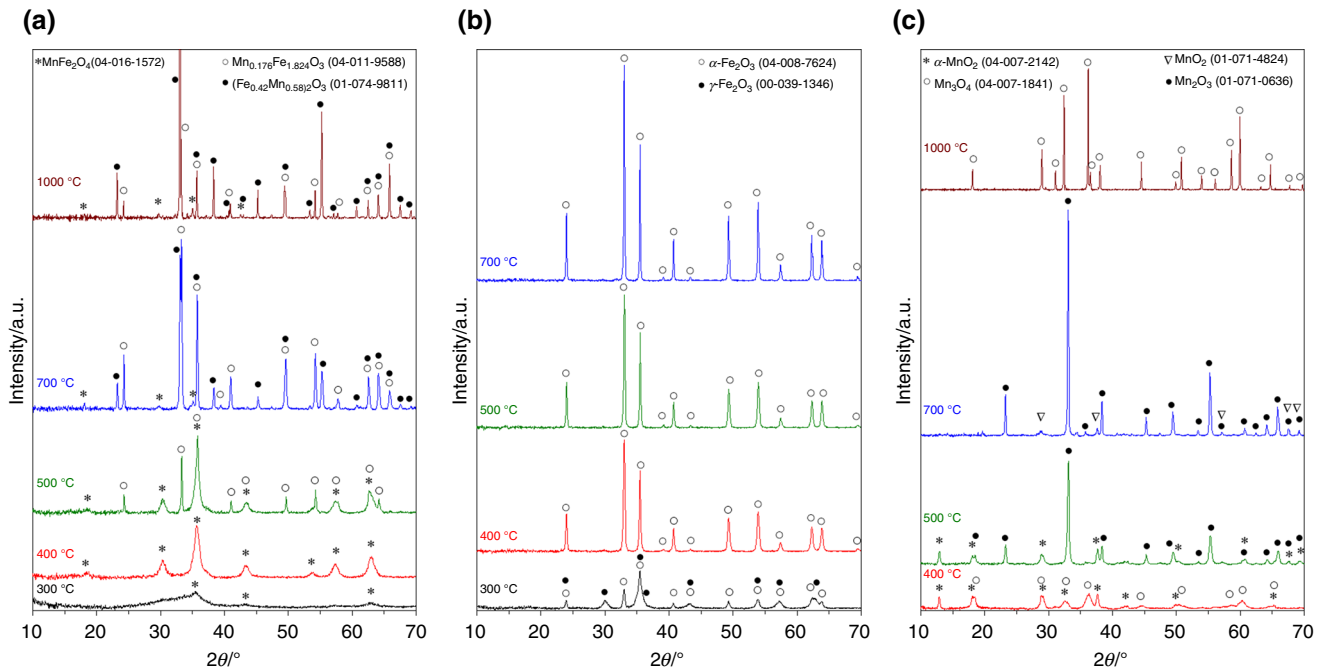

Fig. 4 XRD patterns of samples **a** MnFePVA, **b** FePVA, and **c** MnPVA annealed for 6 h at different temperatures

Table 1 Data derived from XRD analysis

Sample	Temperature/°C	Identified phases	%	*d*/nm	Lattice parameters		
					a/Å	*b*/Å	*c*/Å
MnFePVA	300	$MnFe_2O_4$ Jacobsite, syn	100	2.0	8.333	8.333	8.333
	400	$MnFe_2O_4$ Jacobsite, syn	100	6.1	8.352	8.352	8.352
	500	$Mn_{0.176}Fe_{1.824}O_3$ Manganese Iron Oxide	28	30.3	5.028	5.028	13.720
		$MnFe_2O_4$ Jacobsite, syn	72	8.0	8.360	8.360	8.360
	700	$Mn_{0.176}Fe_{1.824}O_3$ Manganese Iron Oxide	65	66.4	5.035	5.035	13.734
		$(Fe_{0.42}Mn_{0.58})_2O_3$ Bixbyite, ferrian	29	93.2	9.384	9.384	9.384
		$MnFe_2O_4$ Jacobsite, syn	6	7.4	8.498	8.498	8.498
	1,000	$Mn_{0.176}Fe_{1.824}O_3$ Manganese Iron Oxide	25	35.3	5.036	5.036	13.735
		$(Fe_{0.42}Mn_{0.58})_2O_3$ Bixbyite, ferrian	68	117.8	9.411	9.411	9.411
		$MnFe_2O_4$ Jacobsite, syn	7	20.8	8.499	8.499	8.499

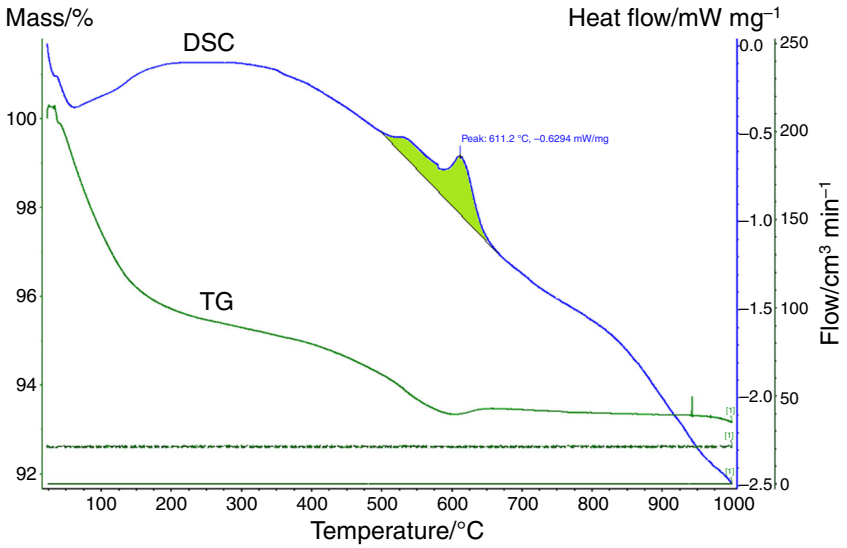

Fig. 5 TG and DSC curves of MnFePVA powder annealed at 400 °C

XRD patterns of MnFePVA sample at 400 °C with the ones of FePVA and MnPVA at the same temperatures, it results that the only possible spinelic phase is $MnFe_2O_4$, as in the same conditions FePVA sample contains only α-Fe_2O_3, and MnPVA sample contains a mixture of two manganese oxides. The absence of any diffraction peaks characteristic to any manganese oxides or α-Fe_2O_3 suggests that in our system manganese ferrite is the formed spinelic phase, even at 300 °C. By raising the calcination temperature at 500 °C, for 6 h, a secondary phase, automatically identified as $Mn_{0.176}Fe_{1.824}O_3$, appears besides the spinelic ferrite. Thus, starting with this temperature manganese ferrite begin to decompose in other phases, probable due to the oxidation of Mn(II) to Mn(III) by the O_2 contained in the oven atmosphere [15]. After annealing at 700 °C, the content of manganese ferrite phase is very low, but there are two crystalline phases, $Mn_{0.176}Fe_{1.824}O_3$ and $(Fe_{0.42}Mn_{0.58})_2O_3$, both containing Mn^{3+}; thus, at this temperature, most of Mn^{2+} ions are oxidized. This is confirmed also by the XRD pattern of the MnPVA sample annealed at 700 °C (Fig. 4c), where Mn_2O_3 is the predominant crystalline phase, contaminated with MnO_2. In the powder annealed at 1,000 °C, the same three crystalline phases are present, but the phase $(Fe_{0.42}Mn_{0.58})_2O_3$ becomes predominant. It can be noticed that the XRD pattern of the MnPVA sample shows that Mn_3O_4 is present as single crystalline phase, thus a part of manganese was reduced at Mn(II).

The decomposition of the manganese ferrite was also evidenced by thermal analysis of sample MnFePVA calcined at 400 °C (Fig. 5). Both TG and DSC curves evidence two thermal processes around 600 °C: one process with a small corresponding mass loss associated with a spread, weak exothermic effect on DSC curve that can be

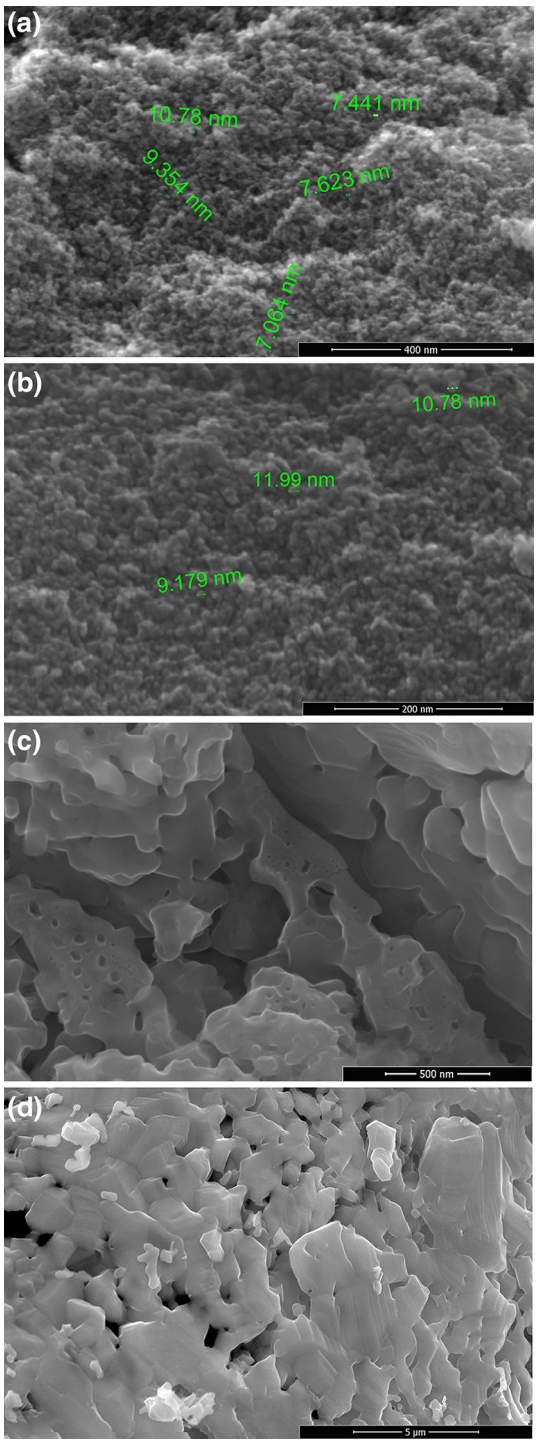

Fig. 6 SEM images of MnFePVA powders calcined at **a** 300 °C; **b** 400 °C; **c** 500 °C; **d** 1,000 °C

by assigned to the burning of residual carbon [29]; the second process with a very small mass gain associated to a sharp but weak exothermic effect suggests that an oxidation takes place. The corresponding temperature (~610 °C) is in agreement with the evolution of crystalline phases derived from the XRD patterns.

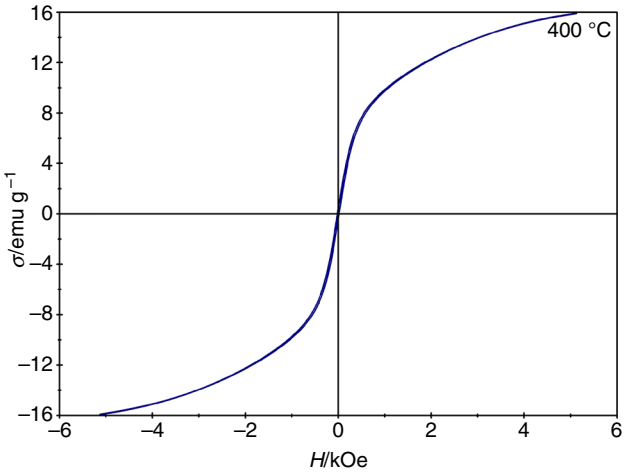

Fig. 7 Magnetization curve for the powder MnFePVA at 400 °C

All powders have been characterized by SEM microscopy in order to study their morphology. Figure 6a–d presents the obtained SEM images. In case of the powders calcined at 300 and 400 °C, fine spherical particles have been obtained, with diameters up to 15 nm, smaller in case of the powder obtained at 300 °C. Due to the fine nature of the particles, the sintering starts even with 500 °C, where a porous mass is obtained. The sintering process is more advanced at 1,000 °C.

The magnetic behavior of the obtained MnFePVA powder showed a significant decrease in saturation magnetization with the increase in annealing temperature above 400 °C, due to the decomposition of manganese ferrite into nonmagnetic phases. The powder obtained at 400 °C exhibits a superparamagnetic behavior (Fig. 7), confirming the fine nature of ferrite nanoparticles. The low value of maximum saturation magnetization reached at a field of 5 kOe (16 emu g^{-1}) is also a consequence of the small size of ferrite nanoparticles [12]. However, this value of saturation magnetization is high enough to insure the possibility of magnetic separation of the powder from a suspension, with a normal magnet.

The powder obtained at 400 °C, which contains manganese ferrite as single crystalline phase was tested as catalyst for the oxidative degradation of phenol. The preliminary catalysis experiments for the degradation of phenol with peroxydisulfate in the presence of manganese ferrite as catalyst evidenced a good catalytic activity of the synthesized nanopowder. High phenol removal efficiency values, above 90 %, have been obtained at pH = 3–3.5, phenol initial concentration around 50 mg L^{-1}, peroxydisulfate–phenol mass ratio of 10:1 and a catalyst dose of 3 g L^{-1}. Total organic carbon measurements showed that the degradation of phenol goes, in these conditions, to mineralization.

Conclusions

Magnetic $MnFe_2O_4$ nanopowder was successfully obtained by a facile synthesis method based on the redox reaction between manganese(II) and iron(III) nitrates and PVA, with formation of a fluffy precursor; the thermal decomposition of this precursor at 400 °C, led to a fine $MnFe_2O_4$ nanopowder. The redox interaction of manganese(II) nitrate, iron(III) nitrate, and of their mixture with PVA was evidenced in the corresponding TG/DTA curves. The complete thermal decomposition of the precursor up to 300 °C allows the obtaining of nanocrystalline manganese ferrite at temperatures below 500 °C, avoiding its decomposition. The oxidation of nanocrystalline manganese ferrite in the range 500–620 °C was evidenced by combined TG/DSC technique, and confirmed by X-ray diffraction. XRD analysis evidenced the presence of $MnFe_2O_4$ as single crystalline phase in the powder calcined at 400 °C. The magnetic powder obtained at 400 °C showed good catalytic activity for the oxidative degradation of phenol in aqueous solutions, in the presence of peroxydisulfate anion as oxidant, so it might be considered a promising nanomaterial for environmental applications.

References

1. Ahmeda MA, El-dek SI, Mansour SF, Okasha N. Modification of Mn nanoferrite physical properties by gamma, neutron, and laser irradiations. Solid State Sci. 2011;13:1180–6.
2. Vamvakidis K, Sakellari D, Angelakeris M, Dendrinou-Samara C. Size and compositionally controlled manganese ferrite nanoparticles with enhanced magnetization. J Nanopart Res. 2013; 15:1743–53.
3. Guan Y-H, Maa J, Ren Y-M, Liu Y-L, Xiao J-Y, Lin L-Q, Zhang C. Efficient degradation of atrazine by magnetic porous copper ferrite catalyzed peroxymonosulfate oxidation via the formation of hydroxyl and sulfate radicals. Water Res. 2013;47:5431–8.
4. Saputra E, Muhammad S, Sun H, Ang H-M, Tadé MO, Wang S. Manganese oxides at different oxidation states for heterogeneous activation of peroxymonosulfate for phenol degradation inaqueous solutions. Appl Catal B. 2013;142–143:729–35.
5. Yang L-X, Wang F, Meng Y-F, Tang Q-H, Liu Z-Q. Fabrication and characterization of manganese ferrite nanospheres as a magnetic adsorbent of chromium. J Nanomater. 2013; ID 293464, http://dx.doi.org/10.1155/2013/293464. Accessed 12 Jan 2015.
6. Sharma US, Sharma RN, Shah R. Physical and magnetic properties of manganese ferrite nanoparticles. Int J Eng Res Appl (IJERA). 2014;4(8):14–7.
7. Kumar AR, Kumar KVGR, Chakra CS, Rao KV. Silver doped manganese–zinc–ferrite nano flowers for biomedical applications. Int J Emerg Technol Adv Eng. 2014;4:209–14.
8. Wang J, Chen Q, Hou B, Peng Z. Synthesis and magnetic properties of single-crystals of $MnFe_2O_4$ nanorods. Eur J Inorg Chem. 2004;6:1165–8.
9. Kedesdy HH, Tauber A. Formation of manganese ferrite by solid-state reaction. J Am Ceram Soc. 1956;39:425–31.
10. Kundu TK, Mishra S. Nanocrystalline spinel ferrites by solid state reaction route. Bull Mater Sci. 2008;31:507–10.
11. Padella F, Alvani C, La Barbera A, Ennas G, Liberatore R, Varsano F. Mechanosynthesis and process characterization of nanostructured manganese ferrite. Mat Chem Phys. 2005;90:172–7.
12. Yang H, Zhang C, Shi X, Hu H, Du X, Fang Y, Ma Y, Wu H, Yang S. Water-soluble superparamagnetic manganese ferrite nanoparticles for magnetic resonance imaging. Biomaterials. 2010;31:3667–73.
13. Wolski W, Wolska E, Kaczmarek J, Piszora P. Formation of manganese ferrite by modified hydrothermal method. Phys Status Solidi. 1995;152:K19–22.
14. Amighian J, Mozaffari M, Nasr B. Preparation of nano-sized manganese ferrite ($MnFe_2O_4$) via coprecipitation method. Phys Status Solidi. 2006;9:3188–92.
15. Deraz NM, Alarif A. Controlled synthesis, physicochemical and magnetic properties of nano-crystalline Mn ferrite system. Int J Electrochem Sci. 2012;7:5534–43.
16. Mathew DS, Juang R-S. An overview of the structure and magnetism of spinel ferrite nanoparticles and their synthesis in microemulsions. Chem Eng J. 2007;129:51–65.
17. Mahmoodi N. Synthesis of amine-functionalized magnetic ferrite nanoparticle and its dye removal ability. J Environ Eng. 2013; 139(11):1382–90.
18. Mahmoodi NM, Arabloo M, Abdi J. Laccase immobilized manganese ferrite nanoparticle: synthesis and LSSVM intelligent modeling of decolorization. Water Res. 2014;67:216–26.
19. Solıs TV, Vigon P, Álvarez S, Marbán G, Fuertes AB. Manganese ferrite nanoparticles synthesized through a nanocasting route as a highly active Fenton catalyst. Catal Commun. 2007;8: 2037–42.
20. Yao Y, Cai Y, Lu F, Wei F, Wang X, Wang S. Magnetic recoverable $MnFe_2O_4$ and $MnFe_2O_4$-graphene hybrid as heterogeneous catalysts of peroxymonosulfate activation for efficient degradation of aqueous organic pollutants. J Hazard Mater. 2014;270:61–70.
21. Mihalca I, Ercuta A. Structural relaxation in $Fe_{70}Cr_{10.5}P_{11.5-}Mn_{1.5}C_{6.5}$ amorphous alloy. J Optoelectron Adv Mater. 2003;5: 245–50.
22. Stoia M, Barbu Tudoran L, Barvinschi P. Nanosized zinc and magnesium ferrites obtained from PVA–metal nitrates' solutions. J Therm Anal Calorim. 2013;113:11–9.
23. Stefănescu M, Stoia M, Stefănescu O, Davidescu C, Vlase G, Sfîrloagă P. Synthesis and characterization of poly(vinylalcohol)/ethylene glycol/silica hybrids. Thermal analysis and FT-IR study. Rev Roum Chim. 2010;55:17–23.
24. Salavati-Niasari M, Davar F, Mazaheri M. Synthesis of Mn_3O_4 nanoparticles by thermal decomposition of a [bis(salicylidiminato)manganese(II)] complex. Polyhedron. 2008;27:3467–71.
25. Ristic M, Music S, Popovic S, Dragcevic D, Marciuš M, Ivanda M. Synthesis and long-term phase stability of $Mn_{-3}O_4$ nanoparticles. J Mol Struct. 2013;1044:255–61.
26. Tang ZX, Sorensen CM, Klabunde KJ, Hadjipanayis GC. Preparation of manganese ferrite fine particles from aqueous solution. J Colloid Interface Sci. 1991;146:38–52.
27. Musat Burojeanu V, Fournés L, Wattiaux A, Etourneau J, Segal E. Cation distribution and magnetic properties of manganese ferrite powder prepared by coprecipitation from MnO_2 and $FeSO_4{\cdot}7H_2O$. Int J Inorg Mater. 2001;3:525–9.
28. Han A, Liao J, Ye M, Li Y, Peng X. Preparation of nano-$MnFe_2O_4$ and its catalytic performance of thermal decomposition of ammonium perchlorate. Chin J Chem Eng. 2011;19:1047–51.
29. Hessien MM, Zaki ZI, Mohsen A-Q. Low-temperature synthesis of nanocrystalline $Mn_{0.2}Ni_{0.8}Fe_2O_4$ by oxalate precursor route. Adv Mater Phys Chem. 2013;3:1–7.